https://doi.org/10.1590/jatm.v14.1252 ORIGINAL PAPER

# Geometric Analysis of Small Wind Turbine Blades Manufactured by Additive Manufacturing

Heitor Andrade Porto[1,*], Carlos Alberto Fortulan[1], Arthur José Vieira Porto[1], Roberto Hideaki Tsunaki[1]

1.Universidade de São Paulo – Escola de Engenharia de São Carlos – São Carlos (SP) – Brazil.

*Correspondence author: heitoraporto@gmail.com

## ABSTRACT

One of the many benefits of additive manufacturing (AM) is to produce parts ready to assemble and use, a concept called direct digital manufacturing (DDM). This, besides the ease of manufacturing complexes geometries, creates a potential for applying the AM technology for producing small wind turbines (SWT) blades. Small wind turbines have an increasing role in the worldwide energy matrix, which can be built up by developing site-optimized and customized turbines. Customizing SWT can increase the energy harvesting potential of such machines; however, it requires flexible manufacturing procedures. The blade's geometric complexity and flexible manufacturing are features that can benefit from the potentials of AM. This work analyses the final geometry of SWT blades manufactured by AM, assessing the scope of DDM in the SWT field. The parts length is 225 mm, the blades were manufactured by the Fused Deposition Modeling (FDM) method using a Dimension Elite machine produced by Stratasys. The geometric evaluation was performed using a CROMA coordinate measuring machine. The measurements showed good results when compared to values adopted in several studies that investigated the effects of geometric disturbances on wind turbine blades. This work affirms that AM is a powerful technology for manufacturing SWT blades in a DDM scope.

**Keywords:** Small wind turbines; Additive manufacturing; Direct digital manufacturing; Geometric analysis.

## INTRODUCTION

Additive manufacturing (AM) holds great potential for an industrial revolution, which has already begun (Comotti *et al.* 2017). From plastics and ceramics to metals, AM can promote the development of complex structures, minimization of waste material, reduction of the need of excessive machine tool operations, optimization of the topology and structure, among other features (Gao *et al.* 2015; Ranjan *et al.* 2017).

A concept called Direct Digital Manufacturing (DDM) was developed based on the several benefits of AM. This concept implies that the parts produced by AM are designed and manufactured directly for using or assembling (Chen *et al.* 2015; Gibson *et al.* 2010). This overtakes the concepts of Design for Manufacturing (DFM) and Design for Assembly (DFA), in which the parts are designed for the ease of machine tool or assembly operations. The DDM concept potentially eliminates the limits for geometric design of engineering parts.

**Received:** Jul. 13, 2021 | **Accepted:** Feb. 24, 2022
**Peer Review History:** Single Blind Peer Review.
**Section editor:** Raj Das

Recently, industries adopted AM not only for producing prototypes but also for manufacturing engineering parts. Engineering parts must have the correct dimensions, geometric tolerances, and mechanical properties to execute the work they were designed for. Hence, AM processes must guarantee the designed dimensions, tolerances, and mechanical properties of such parts. The accurate production of complexes engineering parts and their manufacturing time are still great challenges encountered by AM (Gao *et al.* 2015).

In a continuously changing world, small wind turbines (SWT) present an alternative for the needs of modernizing the worldwide energy matrix, as a way of generating distributed energy (Fields *et al.* 2016; Pitteloud and Gsänger 2017; Tummala *et al.* 2016).

Several studies investigated the state of the SWT technology, most of which depicted the need for improvements (Grieser *et al.* 2015; Sunderland *et al.* 2016; Sessarego and Wood 2015). Among them, one necessary improvement is the need of blades that can respond faster to wind fluctuations; in order words, blades with greater ability of acceleration. A greater ability of acceleration requires a more complex geometry, with higher geometric twist and tapering (Clifton-Smith and Wood 2007; Wood Ebert and Wood 1997; Wright and Wood 2004).

Adding to the necessity of manufacturing complexes blades, another potential application of AM is to increase the flexibility of their production. Small wind turbines blades are mostly made of plastic reinforced with glass fiber which requires the need for a mold. The use of a mold establishes the shape of all the blades to be produced. Given the complex geometry of the blades, the mold becomes the most expensive part of the manufacturing process and its cost restricts the possibility of blade design modifications.

The performance of SWT depends on the wind resource at its deployment site. Different wind resource characteristics will cause different turbine performance (Tang *et al.* 2012), therefore site-optimized blades can impel gains in performance; in other words, more energy conversion. In a mold-oriented production, site optimization is, however, unfeasible. Nonetheless, the broad potentials of AM set up a condition where site-optimized and customized blades could become a reality (Sessarego and Wood 2015).

The potentials of AM and SWT on each particular field added to the need of improvements on the SWT design asks for integrating the technologies, applying AM to develop complexes and customized SWT blades (Akour *et al.* 2018; Bassett *et al.* 2015; Poole and Phillips 2015).

As mentioned, one challenge of AM is to manufacture parts with required geometric tolerances, especially for parts with high geometric complexity, as SWT blades. In the wind energy field, and in aerodynamics in general, geometric variations on aerodynamic surfaces poses a restriction to obtain predicted aerodynamic parameters, causing systems to underperform (Cebeci 1987). Despite the nonexistence of a large amount of data in the literature regarding geometric tolerances on SWT blades manufacturing, it is well known that geometric variations can negatively impact the performance of aerodynamic surfaces (Ernst *et al.* 2014).

In this scope, this work focuses on analyzing the final geometry of SWT blades manufactured by AM, assessing the quality of the AM process and configuration employed for producing the blades.

## EFFECTS OF GEOMETRIC UNCERTAINTY ON AERODYNAMIC PERFORMANCE

To properly evaluate the results of the AM process and configuration adopted for producing the SWT blades, it is first necessary to qualify the effects of geometric disturbances on aerodynamic performance.

Few studies have been published on this topic, which creates an extra difficulty of inferring the results. The fact that the impacts of geometric disturbances on aerodynamic performance are specific to airfoil and working conditions (the Reynolds number and angle of attack) is another complicating issue.

The severe consequences on aerodynamic performance that roughness can cause is widely known. Roughness reduces the maximum lift coefficient value and increases the drag coefficient. Smooth changes in the thickness and camber distribution of an airfoil; however, they do not have a clear impact. They will dislocate the point of minimum pressure, affect the total pressure

distribution over the airfoil and the behavior of the boundary layer but their final impact on the aerodynamic coefficients will be inherent to each specific airfoil and working condition.

Some published studies related to this topic are highlighted in the sequence.

Ernst *et al.* (2014) investigated, through computer simulations, the effects of geometric variations on wind turbine airfoils. The analysis was based on five parameters: maximum thickness, location of the maximum thickness, maximum camber, location of the maximum camber and trailing edge thickness. Before the analysis, the authors highlighted that information about manufacturing tolerances of wind turbine blades is not available in the literature. The applied geometric variations were based on a truncated normal distribution. Except for the trailing edges thickness, the distribution had a mean value of 0 and a standard deviation of 10%. For the trailing edges thickness, the variation limits were set in 100%. This definition was set because of the characteristic small thickness in such position. The calculations of the effects on the lift and drag coefficients of the airfoils were done using XFOIL (Drela 1989) and the simulations were performed at a single Reynolds number. The results showed that the magnitude and characteristics of the effects are inherent to each airfoil and operational condition; in this case, different angles of attack. A high impact on the lift coefficient occurred for an angle of attack near zero and past stall, with the coefficient of variation, for some airfoils, over 0.1. The impacts on the drag coefficient started to be more significant after the angle of attack of 5°, with the coefficient of variation for some airfoils reaching values higher than 0.15.

Petrone *et al.* (2011) studied the effects of geometric uncertainties based on predefined manufacturing tolerances and changes in the airfoil roughness through insect contamination on wind turbine performance. The calculations were also based on computer simulations. The only geometric parameter analyzed considering manufacturing tolerances was the angle of attack of the blade sections, which had the tolerance range defined as 2°. In addition, the authors highlighted the difficulty to characterize the effects of geometric tolerances. The authors analyzed the effects of such parameters directly on the power performance of the wind turbine. A decline in power performance by insect contamination was reported up to 16%, and by the angle of attack manufacturing tolerances up to 7%.

Demuijnck and Kooji (2003) also analyzed the impact of profile deviations, based on computer simulations, on wind turbine airfoils. The deviations were defined in two parts. The first as adding roughness to the airfoils, and the second as thickness increase in the leading and trailing edge of the airfoils. The increase in the thickness normalized to the airfoil's chord was set as 0.54%. The authors found the deviations to have a different impact on the studied airfoils. The simulations on wind turbine performance showed a higher negative impact related to the increase in airfoil roughness, with some cases getting near to 5% in power performance. The thickness variation on the leading and trailing edges had a general impact in power performance less than 1%.

Loeven and Bijl (2008) studied the geometric uncertainties as variations in the maximum camber, maximum camber position, and thickness of a NACA 4-digit series airfoil. All the variables were normalized by the airfoil's chord. The simulations were carried out through computer simulations.

The parameters had a coefficient of variation of 0.1 and were characterized by a truncated normal distribution. The simulations were performed on a fixed Reynolds number. Analyzes of the effects of the parameters occurred separately as well as combined. The critical parameters were the maximum camber and thickness. For the conditions investigated, the coefficient of variation of the aerodynamic coefficients achieved values on the range of 0.15.

The mentioned works highlighted the effects of geometric uncertainties on aerodynamic performance and the lack of information on manufacturing tolerances of wind turbine blades on the open literature. In general, it can be concluded that the impacts are inherent to each airfoil and operational condition (Reynolds number and angle of attack). A common value of 10% for the geometric parameters variation was defined in some analyzes, which resulted in an impact on the final aerodynamic performance. Among the values analyzed, adding roughness on the airfoil's surface was identified as the most critical cause for performance worsening. The works were based on computer simulations and not on experimental data. The authors emphasized the importance of such effects in real life applications and the high negative impact on aerodynamic performance, pointing out the relevance of manufacturing tolerances on the design and production of such parts.

## SWT PARTS PROJECT AND MANUFACTURING

This work is a part of a project that seeks to analyze and optimize the dynamic response (torque and acceleration) of SWT models manufactured by AM.

As previously mentioned, an advantage of using AM is the flexibility and ease to manufacture complexes geometries. With a high geometric and aerodynamic torsion, tapering, winglets, and critical fixing constraints, a wind turbine blade is a complex geometry, therefore an engineering part capable of challenging the potentials of AM. The main parts of the model, blades, nose cone, and hub, were manufactured by AM. This proposal allows evaluating the chosen manufacturing technique, AM, in a DDM scope.

The model is composed of a hub, nose cone, and blades of same geometry, it was designed to have two mounting options, with 3 or 5 blades in the same hub and nose cone (Fig. 1). The blades are not only the most geometrically complex parts, but also the responsible for the basic functioning of the complete machine, their aerodynamic shape produces thrust, torque, and therefore mechanical power. Therefore, the geometric analysis of the manufacturing process and configuration is focused on the blades.

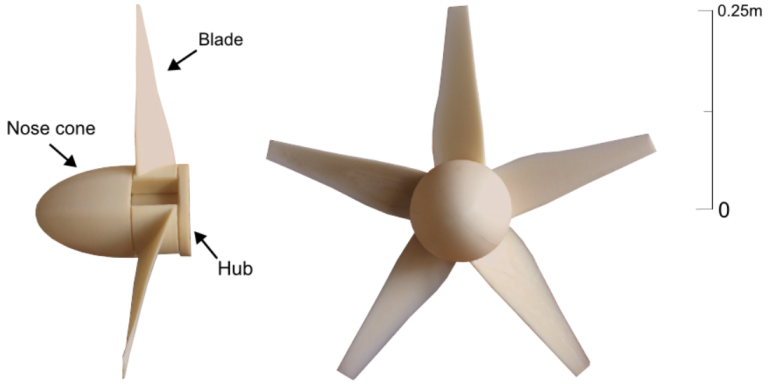


Source: Elaborated by the authors.

**Figure 1.** Three and five blades mounting configurations.

The blades analyzed in this work have no aerodynamic torsion, with the complete span comprised of the SG6043 airfoil (Fig. 2). This is a low Reynolds number airfoil with 10% thickness to chord ratio commonly used for SWT (Giguére and Selig 1998; Wata *et al.* 2011). The blades have a root chord and angle of incidence (in reference to the plane of rotation) of, respectively, 80 mm and 55°, a tip chord and angle of incidence of, respectively, 25 mm and 85°, and a length of 200 mm. The blades dimensions are lower than other SWT blades; nevertheless, they represent a valid condition for geometric analysis of complexes engineering parts in a DDM scope. Further on, the blades were designed connected to their base as one single structure another featured facilitated by AM; the base is then mounted on the hub and nose cone. Apart from the fixing holes, the structure of the blades and the base are solid (Fig. 3). The blades were designed to withstand loads related to a wind speed of 25 mm·s$^{-1}$. In the tests that they have currently undertaken, they withstood loads related to 12 m·s$^{-1}$ wind speed and 1200 rpm.

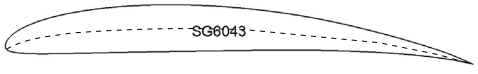


Source: Elaborated by the authors.

**Figure 2.** SG6043 airfoil profile with camber line.

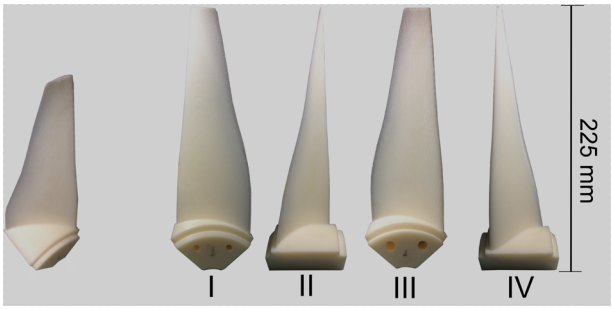


Source: Elaborated by the authors.

**Figure 3.** SWT blade. I. Upper camber view and hub mounting face; II. Lower camber and trailing edge view; III. Lower camber view; IV. Upper camber and leading-edge view.

The manufacturing process of the parts was defined by the use of the Fused Deposition Modeling (FDM) technique in a Stratasys Dimension Elite Machine. The machine has a build size of 203 × 203 × 305 $mm^3$, layer thickness options of 0.178 or 0.254 mm, a heated chamber that minimizes distortions and stress gradients, and the CatalystEX software.

The manufacturing configuration was defined by positioning the blades diagonally on the printing bed: The hub mounting face parallel to the printing bed, the lower camber surface also facing the printing bed and, therefore, in contact with the support material (Fig. 4). The selected layer thickness was 0.254 mm, with the ABS P430 material produced by Stratasys. Each blade took around 20 h to be manufactured.

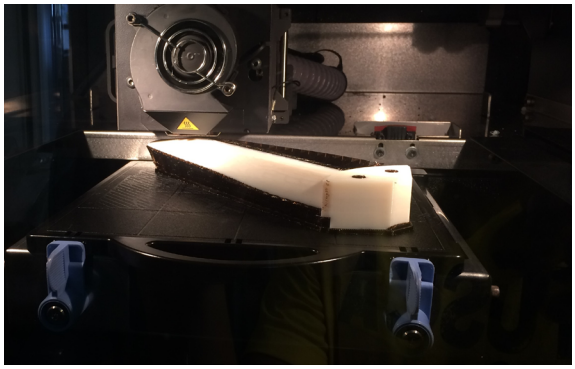

Source: Elaborated by the authors.

**Figure 4.** Manufacturing of the blade. The hub mounting face and lower camber surface are facing the printing bed and are in contact with the support material.

## MEASUREMENT PROCEDURE

The measurements of the SWT blades were done using a Sheffield Croma686 coordinate measuring machine, which provides high-resolution measurements of complexes geometries (Fig. 5). The machine has a scale resolution of 0.078 μm, a measuring volume of 600 × 800 × 600 $mm^3$, a TESASTAR-m motorized probe head, a TESASTAR-mp medium force probe with a 2-mm diameter ruby sphere, and the PC-DMIS 2012 software. The definition of the measurement features such as the approach and touching speed, probe size, and probe joint angles were so to minimize the errors related to such features.

The main goal of the measurements was to analyze the final geometry of the SWT blades in comparison to the reference design model.

The measurements were characterized by defining a reference coordinate axis, dividing the blade into equally spaced sections across its length, and measuring a number of points at each section.

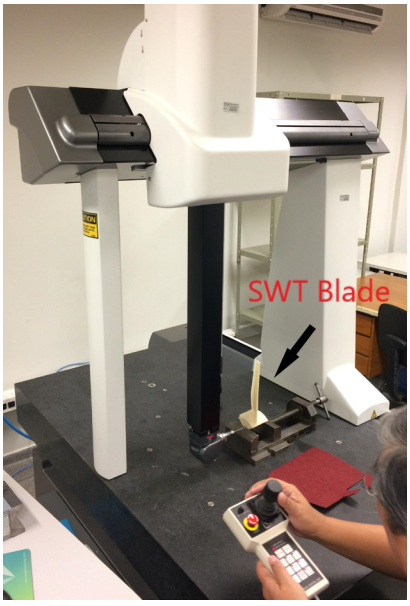


Source: Elaborated by the authors.

**Figure 5.** SWT blade positioned on the measuring machine for the measurement procedure.

The reference axis selected for the measurements was located at the center of one of the two holes used to fix the blade to the hub, projected on the hub mounting face. The blades were divided into ten equally spaced sections across their span, defined in this work as blade sections. Each blade section was then divided into five chord sections, each chord section being comprised of a point in the lower camber and a point in the upper camber surfaces. Therefore, for each blade section, ten points, five in the lower camber and five in the upper camber, were measured. The five chord sections were equally spaced at each blade section. Figure 6 illustrates the described arrangement. The label of the chord sections goes from the leading to the trailing edge, from one to five, while the label of the blade sections goes from the root to the tip, from one to ten.

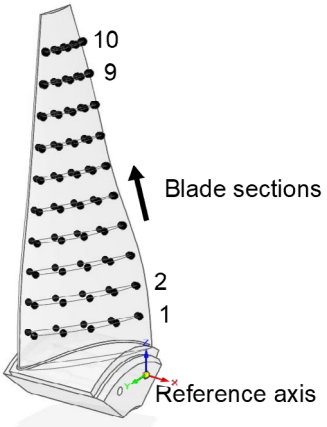


Source: Elaborated by the authors.

**Figure 6.** Illustration of the schematics for the measurement of the blades.

The definition of the geometric variables to be analyzed was based on the main parameters that define an airfoil: the thickness and the camber. Therefore, the geometric parameters analyzed were the thickness of the five chord sections for each of the ten blade sections and the deformation of the camber line of each blade section. Figure 7 illustrates the variables. Besides the thickness and the camber, another parameter analyzed was the angle of incidence of each blade section.

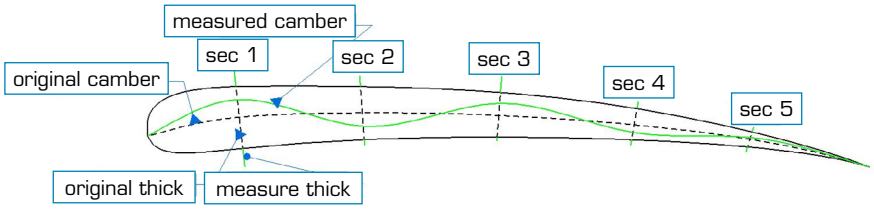


Source: Elaborated by the authors.

**Figure 7.** Illustration of the analyzed geometric variables. Dashed lines illustrate the original variables (camber line and the thickness of the five chord sections). Green lines illustrate possible measured variables. The label of the chord sections goes from the leading to the trailing edge, from one to five.

The camber line deformation analysis was performed by measuring the displacement of each chord section camber line point (middle point of each measured chord section) in reference to the point in the designed model.

The design normalized radial position, chord, angle of incidence values of the ten blade sections and the design thickness of the five chord sections along the ten blade sections are shown in Table 1. Two of the five manufactured blades were randomly selected for the analysis. The results of the measurements are highlighted in the next section.

**Table 1.** SWT design values for the normalized radial position, chord, angle of incidence, and thickness of the five chord sections for the ten blade sections.

| Blade section | Normalized radial position | Chord (mm) | Angle of incidence (degrees) | Thickness of chord sections (mm) | | | | |
|---|---|---|---|---|---|---|---|---|
| | | | | 1 | 2 | 3 | 4 | 5 |
| 1 | 0.100 | 79.5 | 33.00 | 6.245 | 8.024 | 7.312 | 4.873 | 1.630 |
| 2 | 0.189 | 77.6 | 31.17 | 6.096 | 7.832 | 7.137 | 4.756 | 1.591 |
| 3 | 0.278 | 73.3 | 29.54 | 5.758 | 7.398 | 6.741 | 4.493 | 1.503 |
| 4 | 0.367 | 66.4 | 27.86 | 5.216 | 6.702 | 6.107 | 4.070 | 1.362 |
| 5 | 0.456 | 58.6 | 26.05 | 4.603 | 5.914 | 5.389 | 3.592 | 1.202 |
| 6 | 0.545 | 51.8 | 24.31 | 4.069 | 5.228 | 4.764 | 3.175 | 1.062 |
| 7 | 0.634 | 46.4 | 22.83 | 3.645 | 4.683 | 4.267 | 2.844 | 0.952 |
| 8 | 0.723 | 41.5 | 20.93 | 3.260 | 4.189 | 3.817 | 2.544 | 0.851 |
| 9 | 0.811 | 36.4 | 18.10 | 2.859 | 3.674 | 3.348 | 2.231 | 0.747 |
| 10 | 0.900 | 31.0 | 13.36 | 2.435 | 3.129 | 2.851 | 1.900 | 0.636 |

Source: Elaborated by the authors.

## RESULTS AND DISCUSSIONS

The results of the geometric analysis are divided according to the two variables: thickness and camber. The evaluation of the results is based on the studies mentioned in the section "Effects of Geometric Uncertainty on Aerodynamic Performance". Bearing in mind that the effects on aerodynamic performance are inherent to each airfoil and working conditions.

The thickness analysis of the chord sections was done in percentage variation, variation normalized to each blade section chord, and the variation in millimeters. In addition, the points in the upper and lower camber surfaces were analyzed separately. The basis of the analysis of the camber line deformation was the displacement of the chord sections camber line points, in millimeters and normalized to the chord of each blade section. The analysis of the variation of the angle of incidence of the blade section was performed in conjunction with the camber line deformation analysis.

## Thickness variation

The percentage thickness variation of the five chord sections is depicted in Fig. 8. The box plot shows the measured chord sections points dispersion across the ten blade sections. The gray boxes refer to the first blade, while the white boxes refer to the second blade. In addition, for each blade, the blue curve represents the average value of the blade sections 1 and 2, while the red curve represents the average value of the blade sections 9 and 10. Several features can be pointed out from such data and are listed in the sequence.

- For both blades, from chord sections 2 to 4, the percentage value increases, as well as the dispersion;
- For both blades, chord section 1 has a high dispersion with the majority of the points having a negative value;
- Chord section 5 of blade 1 and chord section 1 of blade 2 present errant points;
- For both blades, the value grows from the root to the tip blade sections, with generally the tip blade sections containing the higher values;
- The data show good correlation between the blades.

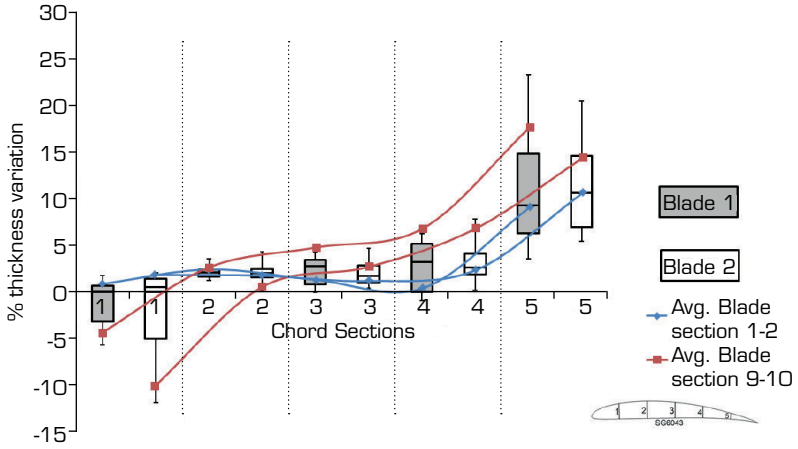


Source: Elaborated by the authors.

**Figure 8.** Boxplot of the percentage variation of the chord sections of both measured blades.

The boxplot depicts the chord sections points dispersion across the blade sections. The gray boxes refer to the first blade, the white boxes refer to the second blade. The blue curves represent the average value of the percentage thickness variation for the blade sections 1 and 2 (root). The red curves represent the average value of the percentage thickness variation for blade sections 9 and 10 (tip).

Comparing to the common 10% value defined in some of the mentioned works in the section "Effects of Geometric Uncertainty on Aerodynamic Performance", the values measured on the blades presented a good result, with the interquartile range inside 5%. The leading and trailing edge are considered, in the mentioned works, regions subjected to higher variations. In the measurements they also presented a higher variation, but with low values when compared with the ones proposed.

In an aerodynamic point of view, it is reasonable to analyze the normalized thickness variation of the chord. This is presented as each chord section thickness variation normalized by their blade section chord.

The following data is shown in Fig. 9, and has the same arrangement as in Fig. 8. Characteristics of the data are listed in the sequence:

- For both blades, from chord section 2 to 4, the percentage value remains somewhat constant, with little variation in the dispersion;
- For both blades, chord section 1 has a higher dispersion with the majority of the points having a negative value;
- Chord section 1 of blade 2 present errant points;
- For both blades, the value grows from the root to the tip blade sections, with generally the tip blade sections containing the higher values;
- All the interquartile values are inside ± 0.4%;
- The data show good correlation between the blades.

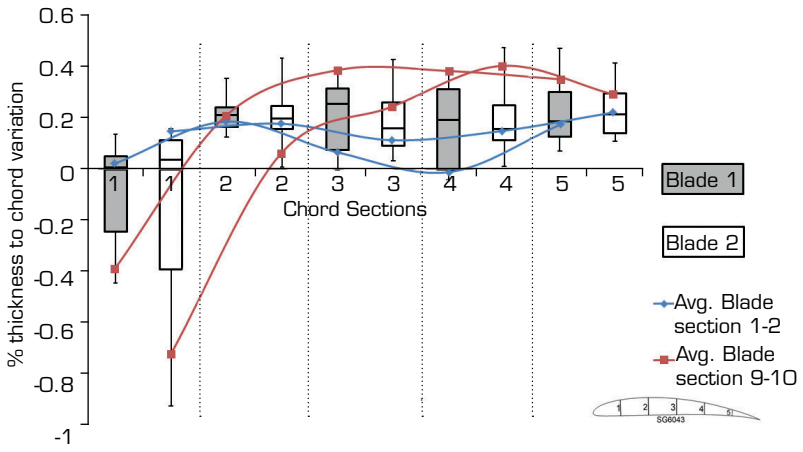


Source: Elaborated by the authors.

**Figure 9.** Boxplot of the percentage thickness to chord variation of the chord sections of both measured blades.

The boxplot depicts the chord sections points dispersion across the blade sections. The gray boxes refer to the first blade, the white boxes refer to the second blade. The blue curves represent the average value of the percentage thickness to chord variation for the blade sections 1 and 2. The red curves represent the average value of the percentage thickness to chord variation for blade sections 9 and 10.

Aerodynamically, it is intricate to affirm the consequences of such thickness to chord variations, as these are not punctual or localized deformations but smooth deviations along the airfoil chord.

Nevertheless, knowing that the aerodynamic performance of the airfoils will somehow be affected, the values encountered on this work for the thickness to chord variation show great accuracy and precision of the manufacturing process and configuration selected.

The data previously presented showed that the normalized thickness variation does not have a clear relation to the chord sections. Therefore, an analysis of the thickness variation in millimeters was performed (Fig 10)—the data on the figure is presented in the same structure as in the previous figures. The following can be pointed out:

- For both blades, from chord sections 2 to 4, the value remains somewhat constant, with little variation in the dispersion;
- For both blades, chord section 1 has a higher dispersion with the majority of the points having a negative value;
- Chord section 1 of blade 2 present errant points;
- For both blades, the values present no clear relation between the blade sections;
- The interquartile values are inside ± 0.15 mm;
- The data show good correlation between the blades.

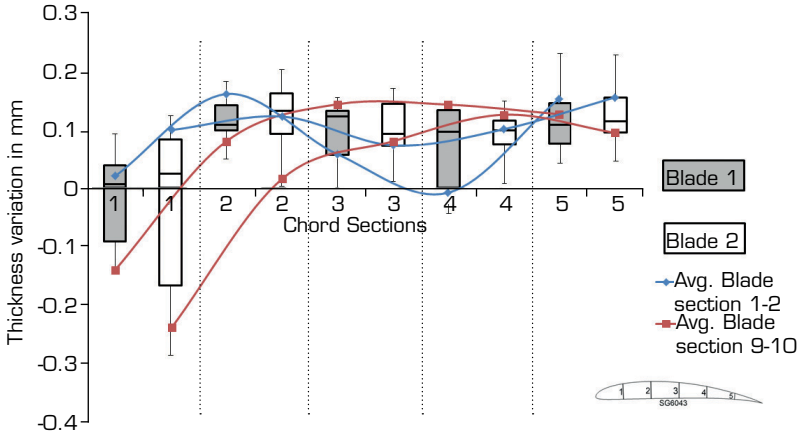


Source: Elaborated by the authors.

**Figure 10.** Boxplot of thickness variation in mm of the chord sections of both measured blades.

The boxplot depicts the chord sections points dispersion across the blade sections. The gray boxes refer to the first blade, the white boxes refer to the second blade. The blue curves represent the average value of the thickness variation, in millimeters, for the blade sections 1 and 2. The red curves represent the average value of the thickness variation, in millimeters, for blade sections 9 and 10.

As expected, the values also presented no clear relation between the chord sections. The value pattern of 0.15 mm explains why the percentage thickness variation (Fig. 8) increases as the chord section thickness decreases (from chord section 2 to 5). This value can be attributed to the manufacturing configuration set for the production of the blades. The choice of a thinner lament diameter could guarantee better geometric accordance with the reference design. However, this decision impacts significantly the total production time, which may also be a constraint during the development of the part. In this case, as in many other AM scenarios, the trade-off between geometric tolerance and production time will determine the optimal configuration.

For a further investigation and understanding of the results, the displacement values of the upper and lower camber points were analyzed separately.

Figure 11 depicts the data for blade 1. The data structure is presented in the same arrangement as in the previous figures, except that now, the gray boxes represent the upper camber surface points and the white boxes the lower camber surface points. The displacement is shown in millimeters. Figure 12 depicts the same data, but for blade 2. The following can be mentioned:

- For both blades, for chord sections 2 to 4, the lower camber points have a higher absolute value;
- For both blades, chord section 1 presents similar displacement values, with the lower camber showing higher dispersion;
- For blade 1, all the values are negative, signaling the displacement was towards the printing bed;
- For blade 1, the displacement showed no clear relation between the blade sections;
- For blade 2, the displacement showed a clear relation between the blade sections. The root sections presented the lower values and the tip sections presented the higher values, indicating a deflection along the blade span;
- For both blades, the upper and lower camber boxes show a similar linear pattern across the chord sections (which is highlighted in the camber line deformation analysis);
- The blades showed correlation on the linear displacement pattern across the chord sections but no correlation on the displacement across the blade sections.

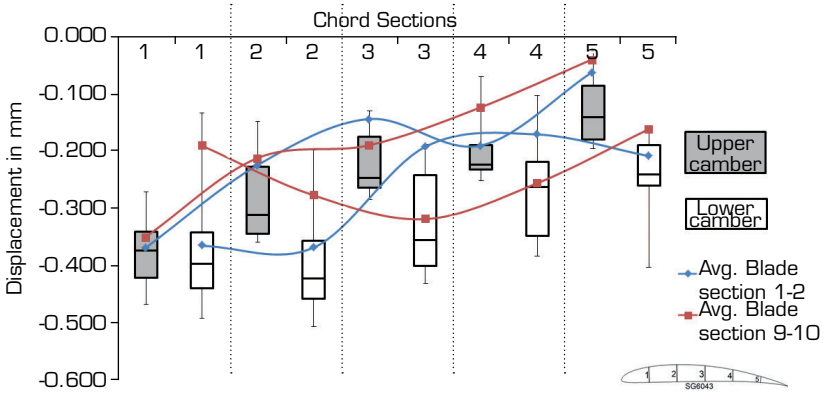


Source: Elaborated by the authors.

**Figure 11.** Boxplot of upper and lower camber point displacement of the chord sections (blade 1).

The boxplot depicts the chord sections points dispersion across the upper and lower camber surfaces for the first blade. The gray boxes refer to the upper camber, the white boxes refer to the lower camber. The blue curves represent the average value of the points displacement in millimeters for blade sections 1 and 2. The red curves represent the average value of the points displacement in millimeters for Blade Sections 9 and 10.

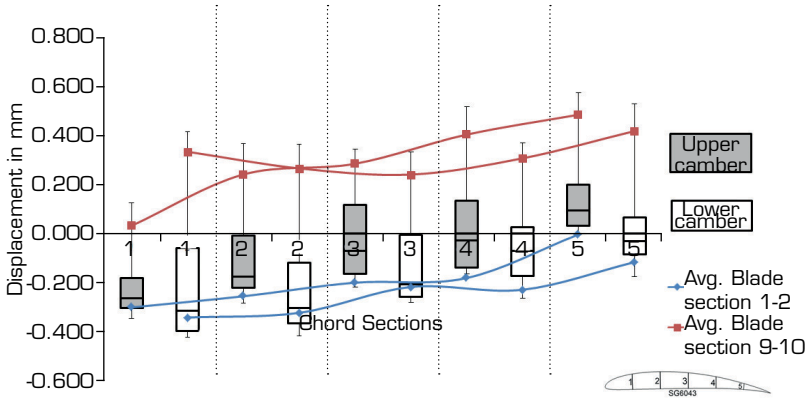


Source: Elaborated by the authors.

**Figure 12.** Boxplot of upper and lower camber point displacement of the chord sections (blade 2).

The boxplot depicts the chord sections points dispersion across the upper and lower camber surfaces for the second blade. The gray boxes refer to the upper camber, the white boxes refer to the lower camber. The blue curves represent the average value of the points displacement, in millimeters, for blade sections 1 and 2. The red curves represent the average value of the points displacement, in millimeters, for blade sections 9 and 10.

The separate analysis of the camber surface points showed the variations of the thickness occurred due to a higher displacement of the lower camber points, which were in contact with the support material, towards the printing bed. The linear pattern presented by the surfaces on both blades gives an insight into the results of the camber line deformation, described in the next section. The displacement values of the camber surface points, for both blades, presented a general direction to the printing bed. This suggests that values can be related to a manufacturing configuration parameter as, for example, the characteristics of the support material and its structure.

In conclusion, the thickness analysis depicted low thickness variation, inside the common 10% values applied in the mentioned works of the section "Effects of Geometric Uncertainty on Aerodynamic Performance". Also, a constant variation value in millimeters, suggesting that the results are highly related to the manufacturing configuration adopted, and finally, a good overall correlation between the blades, highlighting the high precision and accuracy of the manufacturing process and configuration adopted.

## Camber line deformation

The results of the camber line deformation analysis are depicted in the sequence.

The displacement of the camber line points of the first blade is depicted in Fig. 13, and of the second blade in Fig. 14. The data shows the displacement of the camber line points of each chord section at each blade section.

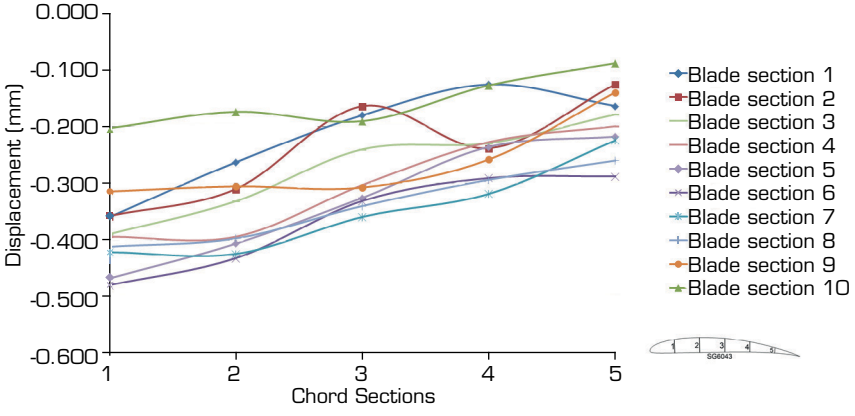


Source: Elaborated by the authors.

**Figure 13.** Displacement of camber chord section points across blade sections (blade 1).

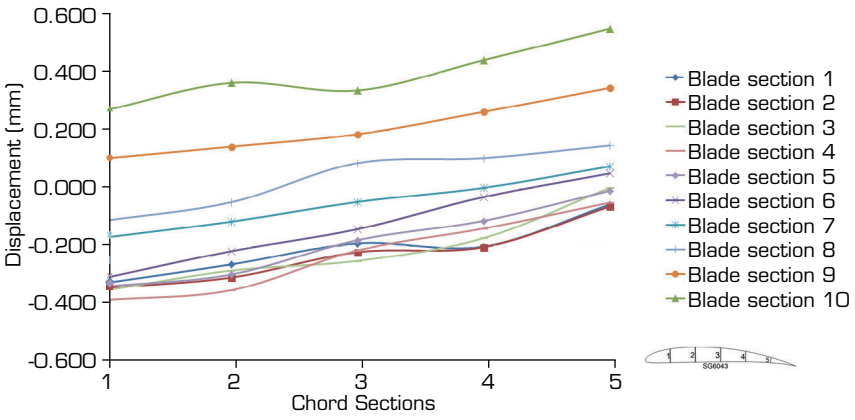


Source: Elaborated by the authors.

**Figure 14.** Displacement of camber chord section points across blade sections (blade 2).

This data correlates to the ones presented in Figs. 11 and 12. Given the similar linear behavior between the two surfaces, the camber points also presented such linear relations. Furthermore, the nonexistent relation across the blade sections for blade 1 and the clear deflection across the blade sections for blade 2, as highlighted in the camber surface points analysis, can be seen. So far, the only noncorrelated behavior between the two blades.

The linear trend was characterized by an angular coefficient and a $R^2$ value. The angular coefficient indicates the inclination of the linear trend and the $R^2$ value the correctness of the linear trend approximation.

The $R^2$ values dispersion for both blades are presented in Fig. 15. Both blades presented values near to 1 and little dispersion, asserting the linear trend. The determination of the angular coefficient allows calculating the variation of the angle of incidence, which is shown in Fig. 16. It can be seen that blade 1 had an angle variation on the range of 0.3° and blade 2 on the range of 0.45°, with blade 2 presenting a higher dispersion across the blade sections.

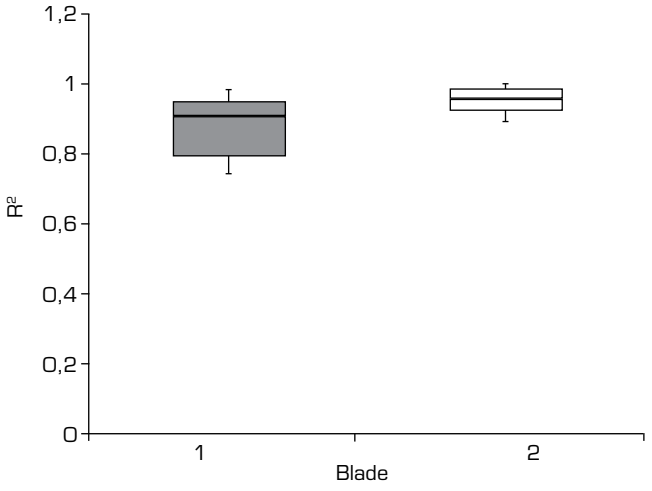


Source: Elaborated by the authors.

**Figure 15.** Boxplot of the $R^2$ values dispersion for blades 1 and 2.

Despite the goodness of the linear approximation presented by the $R^2$ value, there still exists a deformation of the camber line. This deformation was calculated by the Root Mean Square Error (RMSE) of the measured points in relation to the already defined linear trend (Fig. 17). A good correlation between the blades can be seen, with values ranging around 0.025 mm.

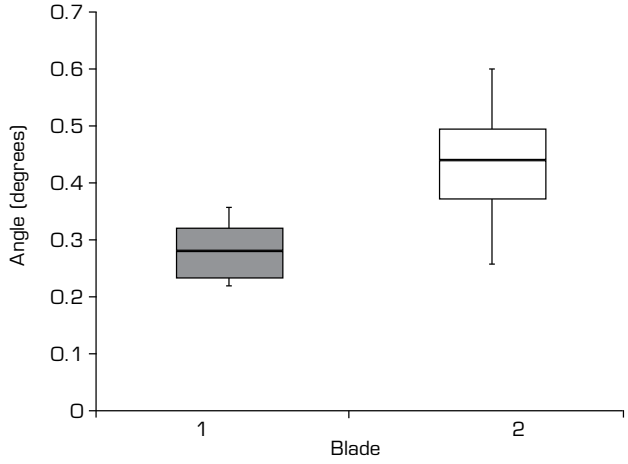


Source: Elaborated by the authors.

**Figure 16.** Boxplot of the angle of incidence values dispersion, in degrees, for blades 1 and 2.

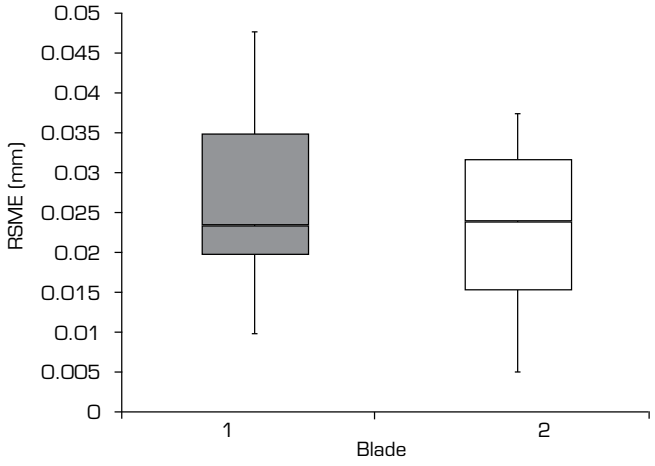


Source: Elaborated by the authors.

**Figure 17.** Boxplot of the RMSE values dispersion, in millimeters, for blades 1 and 2.

The RMSE values were normalized by the chords of each blade section (Fig.18). The final values resulted in a higher upper quartile value of 0.06% and values on the range of 0.045%.

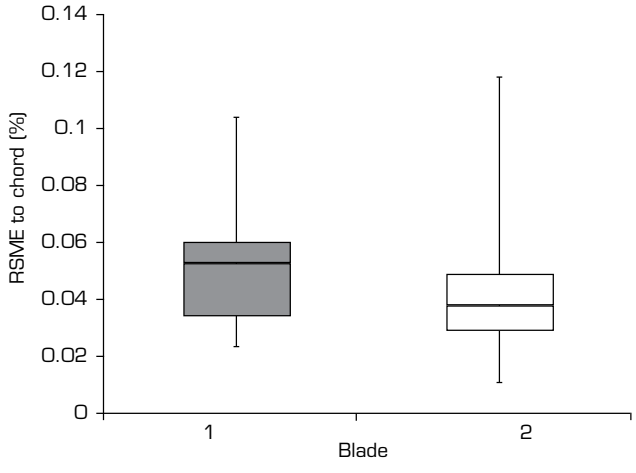


Source: Elaborated by the authors.

**Figure 18.** Box-plot of the RMSE to chord values dispersion, in percentage, for blades 1 and 2.

The camber line deformation analysis showed a good overall correlation between the blades. The camber lines presented minimum deformation. The displacement of the points was translated as a variation of the angle of incidence.

This variation will result in disturbances of the estimated aerodynamic performance but are less than half of the values proposed in the mentioned studies in the section "Effects of Geometric Uncertainty on Aerodynamic Performance". Therefore, the manufacturing process and configuration preserved the camber of the blades sections with high accuracy and precision, with minimal variation of the angle of incidence.

## CONCLUSIONS

This work focused on analyzing the final geometry of an SWT blade produced by AM in a DDM scope. The manufacturing configuration was based on FDM with the ABS P430 material produced by Stratasys and a lament diameter of 0.254 mm. The measurement procedure was conducted using a coordinate measuring machine and analyzed the thickness variation and camber line deformation of the blade sections along the blades span. Two different randomly chosen blades were analyzed in order to assess the accuracy and precision of the manufacturing process and configuration adopted. The results were compared with values assumed in studies in the literature that investigated the effects of geometric disturbances on the aerodynamic performance of wind turbine airfoils.

The results of the geometric evaluation of the blades showed great accuracy and precision of the manufacturing process and configuration adopted. The results of the thickness analysis showed good results when compared with the values proposed in the mentioned works. The thickness normalized to the chord variation interquartile values were inside ± 0.4%. Except for the trailing edge, the interquartile values for the percentage thickness variation of the chord sections of the airfoils were inside 5%. The trailing edge presented interquartile values between 5% and 15%, which are also inside the assumptions made for this chord section on the mentioned works.

Analyzing the thickness variation normalized by the chord of each blade section and the variation in millimeters, a pattern of values not related to the chord sections occurred. This fact allows concluding that this variation may be related to a manufacturing configuration factor, such as the lament diameter, blade positioning, and the support material and its structure. Therefore, a better geometric deviation can be acquired by modifying these parameters; however, this would result in detriments in other factors, such as the manufacturing time. So, a trade-off between geometric tolerances and production time should be accounted for during the definitions of manufacturing configurations of further blades.

The analysis of the camber line deformation showed a low deformation of the camber line of the airfoils. The occurrence of a linear displacement trend was identified, which was translated in a variation of the angle of incidence of the blade sections. However, the values found were considerably lower than the ones proposed by the mentioned works.

Despite the complexities involved in assessing the effects of geometric disturbances on aerodynamic performance, the values found in this study were in accordance with the proposed in the investigations of the mentioned works of the section "Effects of Geometric Uncertainty on Aerodynamic Performance".

The analysis of the measurements performed in this work allows concluding that AM is, in fact, a powerful technology for manufacturing SWT blades. It can also be concluded that the AM technology enables the DDM concept to be applied for manufacturing SWT blades. The merging of these technologies (AM, DDM, and SWT) allows developing site-optimized and customized SWT, enhancing the efficiency of SWT and increasing their strength in the worldwide energy matrix.

Further AM processes and configurations (blade positioning, lament thickness, etc.) should be investigated for producing SWT blades. Future work will also include the analysis of roughness and the necessity of finishing work on the surfaces.

## AUTHORS' CONTRIBUTION

**Conceptualization:** Porto HA; Fortulan CA; Porto AJV; Tsunaki RH; **Methodology:** Porto HA; Porto AJV; Tsunaki RH; **Investigation:** Porto HA; Fortulan CA; Porto AJV; Tsunaki RH; **Writing – Original Draft:** Porto HA; **Writing – Review and Editing:** Porto HA; Fortulan CA; Porto AJV; **Funding Acquisition:** Fortulan CA; **Resources:** Fortulan CA; Porto AJV; Tsunaki RH; **Supervision:** Fortulan CA.

## DATA AVAILABILITY STATEMENT

The data will be available upon request.

## FUNDING

Not applicable.

## ACKNOWLEDGEMENTS

Not applicable.

## REFERENCES

Akour SN, Al-Heymari M, Ahmed T, Khalil KA (2018) Experimental and theoretical investigation of micro wind turbine for low wind speed regions. Renew Energ 116(Part A):215-223. https://doi.org/10.1016/j.renene.2017.09.076

Bassett K, Carriveau R, Ting DS-K (2015) 3D printed wind turbines part 1: Design considerations and rapid manufacture potential. Sustain Energy Technol Assess 11:186-193. https://doi.org/10.1016/j.seta.2015.01.002

Cebeci T (1987) Effects of environmentally imposed roughness on airfoil performance. NASA Contractor Report 179639. NTRS - NASA Technical Reports Server. [accessed Mar 15 2022]. https://ntrs.nasa.gov/search.jsp?R=19890002354

Chen D, Heyer S, Ibbotson S, Salonitis K, Steingrímsson JG, Thiede S (2015) Direct digital manufacturing: definition, evolution, and sustainability implications. J Clean Prod 107:615-625. https://doi.org/10.1016/j.jclepro.2015.05.009

Clifton-Smith MJ, Wood DH (2007) Further dual purpose evolutionary optimization of small wind turbine blades. J Phys Conf Ser 75:012017. https://doi.org/10.1088/1742-6596/75/1/012017

Comotti C, Regazzoni D, Rizzi C, Vitali A (2017) Additive Manufacturing to Advance Functional Design: An Application in the Medical Field. J Comput Inf Sci Eng 17(3):031006. https://doi.org/10.1115/1.4033994

Demuijnck W, Kooij J F (2003) The effect of profile deviations of the DOWEC 6MW blade on wind turbine power production, DOWEC Dutch Offshore Wind Energy Converter project, Task 14 Report DOWEC 10078rev1 (Energy Research Center of the Netherlands).

Drela M (1989) XFOIL: An Analysis and Design System for Low Reynolds Number Airfoils. In: Mueller TJ, editor. Low Reynolds Number Aerodynamics: Proceedings of the Conference Notre Dame, Indiana, USA, 5–7 June 1989. Berlin: Springer. P. 1-12. https://doi.org/10.1007/978-3-642-84010-4_1

Ebert PR, Wood DH (1997) Observations of the starting behavior of a small horizontal axis wind turbine. Renew Energ 12(3):245-257. https://doi.org/10.1016/s0960-1481(97)00035-9

Ernst B, Schmitt H, Seume JR (2014) Effect of Geometric Uncertainties on the Aerodynamic Characteristic of Offshore Wind Turbine Blades. J Phys Conf Ser 555:012033. https://doi.org/10.1088/1742-6596/555/1/012033

Fields J, Oteri F, Preus R, Baring-Gould I (2016) Deployment of Wind Turbines in the Built Environment: Risks, Lessons, and Recommended Practices. National Renewable Energy Lab. (NREL), Golden, CO (United States). Report No.: NREL/TP-5000-65622. https://doi.org/10.2172/1260340

Gao W, Zhang Y, Ramanujan D, Ramani K, Chen Y, Williams CB, Wang CCL, Shin YC, Zhang S, Zavattieri PD (2015) The status, challenges, and future of additive manufacturing in engineering. Comput Aided Des 69:65-89. https://doi.org/10.1016/j.cad.2015.04.001

Gibson I, Rosen DW, Stucker B (2010) Additive Manufacturing Technologies. Boston: Springer. https://doi.org/10.1007/978-1-4419-1120-9

Giguére P, Selig MS (1998) New airfoils for small horizontal axis wind turbines. J Sol Energy Eng 120(2):108-114. https://doi.org/10.1115/1.2888052

Grieser B, Sunak Y, Madlener R (2015) Economics of small wind turbines in urban settings: An empirical investigation for Germany. Renew Energ 78:334-350. https://doi.org/10.1016/j.renene.2015.01.008

Loeven A, Bijl H (2008) Airfoil Analysis with Uncertain Geometry Using the Probabilistic Collocation Method. Paper presented 49th AIAA/ASME/ASCE/AHS/ASC Structures, Structural Dynamics, and Materials Conference. American Institute of Aeronautics and Astronautics, Schaumburg, United States. https://doi.org/10.2514/6.2008-2070

Petrone G, Nicola C, Quagliarella D, Witteveen J, Iaccarino G (2011) Wind Turbine Performance Analysis Under Uncertainty. Paper presented 49th AIAA Aerospace Sciences Meeting including the New Horizons Forum and Aerospace Exposition. American Institute of Aeronautics and Astronautics, Orlando, United States. https://doi.org/10.2514/6.2011-544

Pitteloud J-D, Gsänger S (2017) Small Wind World Report Summary. World Wind Energy Association (WWEA), Bonn (Germany). [accessed Mar 15 2022]. http://www.wwindea.org/download/SWWR2017-SUMMARY(2).pdf

Poole S, Phillips R (2015) Rapid prototyping of small wind turbine blades using additive manufacturing. Paper presented 2015 Pattern Recognition Association of South Africa and Robotics and Mechatronics International Conference (PRASA-RobMech). IEEE; Port Elizabeth, South Africa. https://doi.org/10.1109/robomech.2015.7359521

Ranjan R, Samant R, Anand S (2017) Integration of design for manufacturing methods with topology optimization in additive manufacturing. J Manuf Sci Eng 139(6):061007. https://doi.org/10.1115/1.4035216

Sessarego M, Wood D (2015) Multi-dimensional optimization of small wind turbine blades. Renewables: Wind, Water, and Solar 2(1):9. https://doi.org/10.1186/s40807-015-0009-x

Sunderland KM, Narayana M, Putrus G, Conlon MF, McDonald S (2016) The cost of energy associated with micro wind generation: International case studies of rural and urban installations. Energy 109:818-829. https://doi.org/10.1016/j.energy.2016.05.045

Tang C, Soong WL, Freere P, Pathmanathan M, Ertugrul N (2012) Dynamic wind turbine output power reduction under varying wind speed conditions due to inertia. Wind Energy 16(4):561-573. https://doi.org/10.1002/we.1507

Tummala A, Velamati RK, Sinha DK, Indraja V, Krishna VH (2016) A review on small scale wind turbines. Renew Sust Energ Rev 56:1351-1371. https://doi.org/10.1016/j.rser.2015.12.027

Wata J, Faizal M, Talu B, Vanawalu L, Sotia P, Ahmed MR (2011) Studies on a low Reynolds number airfoil for small wind turbine applications. Sci China Technol Sci 54(7):1684-1688. https://doi.org/10.1007/s11431-011-4411-3

Wright AK, Wood DH (2004) The starting and low wind speed behaviour of a small horizontal axis wind turbine. J Wind Eng Ind Aerodyn 92(14-15):1265-1279. https://doi.org/10.1016/j.jweia.2004.08.003